Human Molecular Genetics, 2007, Vol. 16, No. 24 **2991–3001**
doi:10.1093/hmg/ddm257
Advance Access published on September 12, 2007

Mtmr13/Sbf2-deficient mice: an animal model for CMT4B2

Kristian Tersar[1†], Matthias Boentert[2†], Philipp Berger[1,3], Sonja Bonneick[1], Carsten Wessig[4], Klaus V. Toyka[4], Peter Young[2] and Ueli Suter[1*]

[1]Institute of Cell Biology, Department of Biology, ETH Zürich, Switzerland, [2]Department of Neurology and Interdisciplinary Center of Clinical Research, University of Münster, Münster, Germany, [3]Molecular Cell Biology, Paul Scherrer Institut, Villigen, Switzerland and [4]Department of Neurology, University of Wurzburg, Würzburg, Germany

Received July 12, 2007; Revised and Accepted September 4, 2007

Charcot-Marie-Tooth (CMT) disease denotes a large group of genetically heterogeneous hereditary motor and sensory neuropathies and ranks among the most common inherited neurological disorders. Mutations in the Myotubularin-Related Protein-2 (*MTMR2*) or MTMR13/Set-Binding Factor-2 (*SBF2*) genes are associated with the autosomal recessive disease subtypes CMT4B1 or CMT4B2. Both forms of CMT share similar features including a demyelinating neuropathy associated with reduced nerve conduction velocity (NCV) and focally folded myelin. Consistent with a common disease mechanism, the homodimeric MTMR2 acts as a phosphoinositide D3-phosphatase with phosphatidylinositol (PtdIns) 3-phosphate and PtdIns 3,5-bisphosphate as substrates while MTMR13/SBF2 is catalytically inactive but can form a tetrameric complex with MTMR2, resulting in a strong increase of the enzymatic activity of complexed MTMR2. To prove that MTMR13/SBF2 is the disease-causing gene in CMT4B2 and to provide a suitable animal model, we have generated *Mtmr13/Sbf2*-deficient mice. These animals reproduced myelin outfoldings and infoldings in motor and sensory peripheral nerves as the pathological hallmarks of CMT4B2, concomitant with decreased motor performance. The number and complexity of myelin misfoldings increased with age, associated with axonal degeneration, and decreased compound motor action potential amplitude. Prolonged F-wave latency indicated a mild NCV impairment. Loss of Mtmr13/Sbf2 did not affect the levels of its binding partner Mtmr2 and the Mtmr2-binding Dlg1/Sap97 in peripheral nerves. Mice deficient in *Mtmr13/Sbf2* together with known *Mtmr2*-deficient animals will be of major value to unravel the disease mechanism in CMT4B and to elucidate the critical functions of protein complexes that are involved in phosphoinositide-controlled processes in peripheral nerves.

INTRODUCTION

Charcot-Marie-Tooth (CMT) disease, also called hereditary motor and sensory neuropathies (HMSN), comprise a genetically heterogeneous group of inherited disorders affecting myelinated axons in the peripheral nervous system (1–3) with a prevalence of approximately 1:2500 (4). The disease is characterized by progressive distally accentuated muscle weakness and atrophy. Based on clinical, electrophysiological, and histological data, CMT has been subdivided into demyelinating and axonal forms. Demyelinating neuropathies are diagnosed by reduced nerve conduction velocity (NCV). Axonal loss and muscle atrophy are also observed most likely as secondary effects due to the tight interaction and communication between myelinating Schwann cells, axons and muscle cells (5). Axonal forms of CMT are characterized by a reduction of the compound muscle action potential (CMAP) amplitude due to a loss of myelinated axons (6). Dissection of the cellular functions of the gene products altered in CMT as well as the generation of detailed pathophysiological models are of crucial importance to understand the underlying common as well as distinct disease mechanisms which may affect Schwann cells, axons or both (2).

*To whom correspondence should be addressed. Institute of Cell Biology, ETH Hönggerberg, CH-8093 Zürich, Switzerland. Tel: +41 446333432; Fax: +41 446331190; Email: usuter@cell.biol.ethz.ch
†The authors wish it to be known that, in their opinion, the first two authors should be regarded as joint First Authors.

The subtype CMT4B is a severe demyelinating autosomal recessive inherited neuropathy with onset in early childhood. Histological analysis of human nerve biopsies revealed demyelination and focally folded myelin as the particular pathological hallmark (7). The disease was mapped to chromosome 11q22 and 11p15 indicating that mutations in two different genes lead to indistinguishable pathologies (8–10). Further mapping refinements and molecular cloning lead to the identification of *Myotubularin-Related-Protein-2 (MTMR2)* and *MTMR13/Set-Binding-Factor-2 (SBF2)* as the disease causing genes of CMT4B1 and CMT4B2 (11–13). *Mtmr2*-deficient mice have been generated and mimic the pathology of CMT4B1 closely (14,15).

MTMR2 and MTMR13/SBF2 belong to the family of myotubularin-related proteins (16). This family consists of 14 members in human and orthologues have been found throughout the eukaryotic kingdom but not in bacteria. Myotubularin, the founding member of the family, has been originally identified as the disease-causing gene in X-linked myotubular myopathy (17). The domain signature of MTMRs is defined by the presence of a phospoinositide (PI)-binding PH-GRAM (pleckstrin homology-glucosyltransferases, Rab-like GTPase activators and myotubularins)-homology domain, a phosphatase domain, and a coiled coil motif. The phosphatase domain was initially described as a potential protein tyrosine/dual specific phosphatase, but the PIs (PtdIns)-3-phosphate (P) and PtdIns-3,5-P2 (with myotubularin phosphatase activity specific for the D3 position of the inositol ring) have emerged as the main substrates (16,18). The membrane-associated PtdIns-3-P and PtdIns-3,5-P2 regulate trafficking in the endosomal–lysosomal pathway suggesting that the disease mechanisms in MTMR-based diseases are likely to be related to these processes. Interestingly, disturbances of regulatory mechanisms involving PIs seem to become a recurrent theme in CMT since mutations in FIG4, a D5 phosphatase using PtIns-3,5-P2 as substrate, have been recently described to cause CMT4J (19).

Six members of the myotubularin family, including MTMR13/SBF2, contain inactivating substitutions in the phosphatase domain. Catalytically inactive MTMRs can interact with active MTMRs as modulators of the phosphatase activity, substrate traps or they influence the subcellular localization. Specifically and in addition to the common motifs, MTMR13/SBF2 contains a classical PtIns-3,4,5-P3-binding PH domain (20), a DENN (differentially expressed in normal versus neoplastic) domain and a stretch of 500 amino acids with no homologies to other proteins (Fig. 1A). MTMR13/SBF2 exists in cells independently as a homodimer, as well as in complex with a homodimer of MTMR2 (20–22). The latter association dramatically increases the enzymatic activity of the binding partner MTMR2 (20).

Here, we have generated *Mtmr13/Sbf2*-deficient and *Mtmr2//Mtmr13/Sbf2* double-deficient mice to dissect the role of this pair of myotubularins in health and disease *in vivo*.

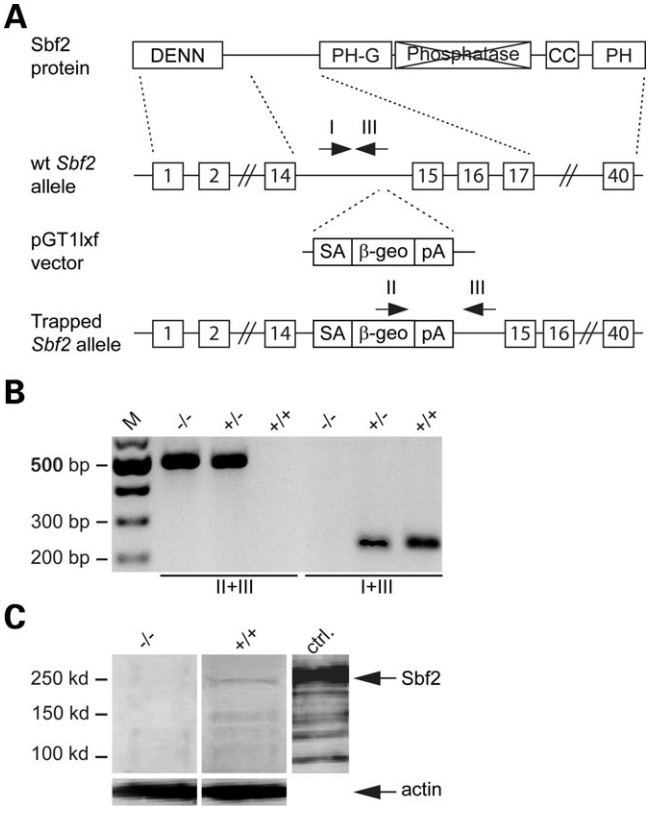

Figure 1. Gene trapped disruption of *Mtmr13/Sbf2*. (**A**) Ideogram of the Mtmr13/Sbf2 protein structure (first row) and the *Mtmr13/Sbf2* gene (second row). The gene trap vector and the locus of the gene-trap integration into intron 14 of *Mtmr13/Sbf2* is schematically depicted in rows three and four, respectively. Arrows marked with I and II represent the forward primers for the wt and trapped *Mtmr13/Sbf2* alleles, respectively, and III the reverse primer for the genotyping PCR (SA, splice acceptor; beta-geo, beta-galactosidase and neomycin-resistance fusion gene; pA, polyadenylation site). (**B**) Genotyping PCR for homozygous (−/−), or heterozygous (+/−) *Mtmr13/Sbf2* mutant mice, or wt (+/+). (**C**) Western blot analysis of sciatic nerve lysates of *Mtmr13/Sbf2*-deficient (−/−) and wt (+/+) control mice. A rabbit polyclonal antibody was used to detect the 210 kDa Mtmr13/Sbf2 protein. Purified CBP-tagged Mtmr13/Sbf2 protein from a baculovirus expression system served as positive control (20). Bands below 210 kDa represent degradation products of Mtmr13/Sbf2.

RESULTS

Gene-trapped disruption of *Mtmr13/Sbf2*

We have used mouse embryonic stem cells carrying a gene trap insertion in the *Mtmr13/Sbf2* locus (XH212; Baygenomics Gene Trap Resource) for the generation of an *Mtmr13/Sbf2*-deficient mutant mouse line using established procedures (15). The insertion site of the gene trap cassette was mapped 1267 bp downstream of exon 14 of *Mtmr13/Sbf2* (Fig. 1A). Based on this information, primers I, II and III were designed to discriminate between different alleles and for genotyping (Fig. 1B). Western-blot analysis of sciatic nerve lysates of *Mtmr13/Sbf2*-deficient and wt littermates revealed that the Mtmr13/Sbf2 protein was absent (Fig. 1C). Mice with a disrupted *Mtmr13/Sbf2* allele are viable and were born according to Mendelian expectations. No obvious sings of impaired spermatogenesis were observed in contrast to some *Mtmr2* mutants (14). Having this viable *Mtmr13/Sbf2* allele at hand, we generated also *Mtmr2//Mtmr13/Sbf2*-double deficient mice by appropriate cross breeding with *Mtmr2*-deficient mutant animals (15). These *Mtmr2//Mtmr13/Sbf2*-double deficient mice were also viable and born according to Mendelian

ratios. Upon visual inspection, the behavioral phenotype of both *Mtmr13/Sbf2*-deficient and *Mtmr2//Mtmr13/Sbf2*-double deficient mice appeared normal compared to control littermates. Starting at the age of 2 months, however, both mutant lines showed an unusual but very mild hind limb clamping upon tail suspension (data not shown). Double-heterozygous *Mtmr2//Mtmr13/Sbf2* mutant animals appeared indistinguishable from their wt littermates up to 15 months of age (latest time point examined).

Expression analysis of Mtmr2, Mtmr13/Sbf2 and Dlg1/Sap97 in sciatic nerves of mutant animals

In a first step, we analysed whether alterations in Mtmr2 or Mtmr13/Sbf2 expression alter the protein levels of its respective binding partner in the sciatic nerve of mutant animals. Western blot analysis of sciatic nerve lysates from 12-month-old animals revealed that Mtmr2 levels were unchanged in *Mtmr13/Sbf2*-deficient mice (Fig. 2A). Vice versa, Mtmr13/Sbf2 levels remained unaltered in *Mtmr2*-deficient mice (Fig. 2B). Bolino *et al*. (14) and Bolis *et al*. (23) have reported an interaction of Mtmr2 with Sap97. They detected also reduced expression of Sap97 in the sciatic nerves of their strain of *Mtmr2*-deficient mice. Here, we confirmed these findings in our strain of *Mtmr2*-mutant mice (15). We continued to test whether loss of Mtmr13/Sbf2 would also reduce the levels of Sap97 by reasoning that loss of the Mtmr2 interaction partner Mtmr13/Sbf2 might affect indirectly the interaction between Mtmr2 and Sap97 within a putative larger complex. However, the levels of Sap97 were not significantly different to wt in *Mtmr13/Sbf2*-deficient mice (Fig. 2C). Consistent with these findings, we found a comparable reduction of Sap97 in *Mtmr2//Mtmr13/Sbf2*-double deficient mice as in *Mtmr2*-single mutants (Fig. 2D). We conclude that the interaction of Mtmr13/Sbf2 with Mtmr2 and the interaction between Mtmr2 and Sap97 are unlikely to be intimately connected. This conclusion was also supported by co-immunoprecipitation experiments revealing no apparent differences in the interaction of Mtmr2 with Sap97 between wt and *Mtmr13/Sbf2*-deficient sciatic nerves (data not shown).

Behavioral analysis

Visual examination of both *Mtmr13/Sbf2*-deficient and *Mtmr2//Mtmr13/Sbf2*-double-deficient mice revealed no obvious signs of tremor or major functional disability, similar to what we had observed in the *Mtmr2*-deficient model of CMT4B1 (15). Therefore, we performed a rotarod test to assess whether a behavioral difference related to motor function was detectable using this assay. At the age of 4 months, *Mtmr13/Sbf2*-deficient mice were not distinguishable from wt mice (Fig. 3A). At 12 months of age, however, *Mtmr13/Sbf2* mutant animals showed a significantly reduced performance compared to their wt control littermates (Fig. 3B) and similar results were obtained with *Mtmr2//Mtmr13/Sbf2*-double-deficient mice (Fig. 3C). No significant difference between the two mutant strains was observed. Based on the results at this point, we decided not to perform further detailed studies on *Mtmr2//Mtmr13/Sbf2*-double deficient mice. Qualitatively, we did not observe major pathology differences compared to the single *Mtmr13/Sbf2* mutants (data not shown).

Electrophysiology of peripheral nerves of *Mtmr13/Sbf2*-deficient mice

Motor nerve conduction of sciatic nerves was studied in *Mtmr13/Sbf2*-deficient mice at the age of 4 and 12 months (Fig. 4). In 4-month-old animals, the CMAP amplitude was not significantly different in *Mtmr13/Sbf2*-deficient mice compared to wt (18.0 ± 3.7 versus 14.0 ± 3.6 mV). At 12 months of age, however, *Mtmr13/Sbf2*-deficient mice showed a significant reduction of the CMAP (7.3 ± 1.1 versus 16.3 ± 2.2 mV in wt mice) and a slightly prolonged F-wave latency of 5.1 ± 0.2 ms (4.4 ± 0.1 ms in wt). Such a very mildly prolonged F-wave latency was already present in 4-month-old *Mtmr13/Sbf2*-deficient animals (4.7 ± 0.2 versus 4.2 ± 0.2 ms in wt). A tendency towards NCV slowing was not significant at both ages examined.

Progressive myelin abnormalities in peripheral nerves of *Mtmr13/Sbf2*-deficient mice

Focally folded myelin is the histological hallmark of both CMT4B1 and CMT4B2. Thus, we focused our analysis on the presence, time course and distribution of focal dysmyelination. At 4 months of age, *Mtmr13/Sbf2*-deficient mice showed numerous sciatic nerve fibres with focally folded myelin (Fig. 5). Abnormalities included both infoldings and outfoldings of the entire myelin sheath which particularly affected large calibre fibres but also smaller, thinly myelinated fibres. Non-myelinated fibres appeared normal. At higher magnification, sciatic nerve cross sections of mutant mice were littered with various degrees of dysmyelination ranging from focal budding of the myelin sheath to multiple or combined infoldings and outfoldings.

Abnormal myelin structures were first but rather sporadically observed in the sciatic nerves of *Mtmr13/Sbf2*-deficient mice already at the age of 3 weeks (Fig. 6A and B). Irregular myelin folds were easily detectable although of low complexity. Quantitative analysis of these pathological structures revealed a significant increase in numbers compared to wt animals (Fig. 7A). Next, since CMT is usually associated with a clinically progressive time course, we followed the qualitative and quantitative progression of the pathology over time. Thus, we examined sciatic nerves at the age of 4 and 15 months (Fig. 6C–F; Fig. 7A). We found a progressive increase in both, the complexity (age-dependent tendency to double and multiple infoldings and outfoldings) as well as the number of misfolded myelin sheaths in *Mtmr13/Sbf2*-deficient animals suggesting that the disease process is continuous throughout the timeframe analysed. Particularly in older mice, some signs of axonal damage were recognized although we did not observe an obvious major loss of myelinated axons. Next we reasoned, considering the suggested molecular function of myotubularins, that the misfoldings of myelin observed in *Mtmr13/Sbf2*-deficient mice might be due to altered vesicular trafficking and myelin-membrane overgrowth. This could potentially lead to generally altered myelin sheath thickness as we have observed in myelin

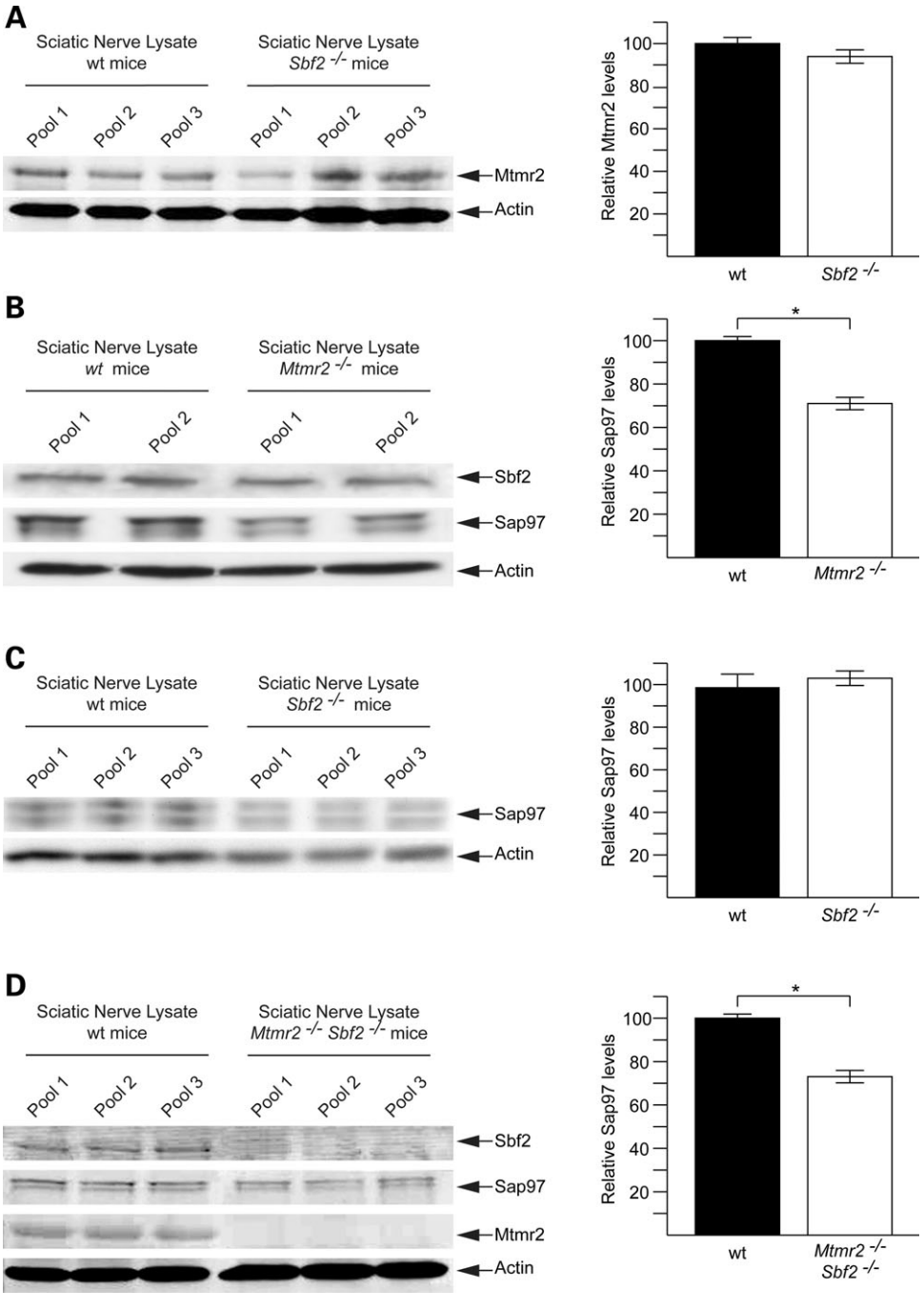

Figure 2. Western blot analysis of the relative Mtmr13/Sbf2, Mtmr2 and Dlg1/Sap97 levels in sciatic nerve lysates from 12-month-old wt, *Mtmr2*-deficient *(Mtmr2−/−)*, *Mtmr13/Sbf2*-deficient *(Sbf2−/−)* and *Mtmr2//Mtmr13/Sbf2*-double deficient *(MTMR2−/− Sbf2−/−)* mice. Each pool contains the sciatic nerves from two or three animals. Protein levels of Mtmr13/Sbf2, Mtmr2 and Sap97 were quantified by normalizing the relative protein levels to beta-actin, illustrated in a bar chart. (**A**) The relative protein level of Mtmr2 does not differ significantly between wt and *Mtmr13/Sbf2*-deficient *(Sbf2−/−)* sciatic nerves. (**B**) The Mtmr13/Sbf2 expression level shows no difference in *Mtmr2*-deficient *(Mtmr2−/−)* compared to wt control lysates of sciatic nerves. The Sap97 protein levels in *Mtmr2*-deficient *(Mtmr2−/−)* lysates are significantly reduced ($P < 0.05$, Student's *t*-test). (**C**) The relative protein level of Sap97 protein level is not altered in the lysates of *Mtmr13/Sbf2*-deficient *(Sbf2−/−)* mice compared to wt control lysates. (**D**) The relative protein levels of Mtmr13/Sbf2, Sap97 and Mtmr2 were compared in wt and *Mtmr2//Mtmr13/Sbf2*-double deficient *(MTMR2−/− Sbf2−/−)* sciatic nerves. As expected, no expression of Mtmr13/Sbf2 or Mtmr2 protein was found. The Sap97 protein is significantly reduced compared to wt ($P < 0.05$; Student's *t*-test) in the lysates of the double mutant mice. Error bars indicate the SEM.

mutants with multi-folded myelin extensions in the central nervous system (24). However, using computer-aided morphometry, we did not detect significant alterations in myelin thickness and axon diameter in *Mtmr13/Sbf2*-deficient sciatic nerves (Fig. 7B and C), consistent with our identical previous findings in *Mtrm2*-deficient mice (15). In agreement with these data, we did not observe Schwann cell onion bulb formation as the classical indicators of demyelination and remyelination.

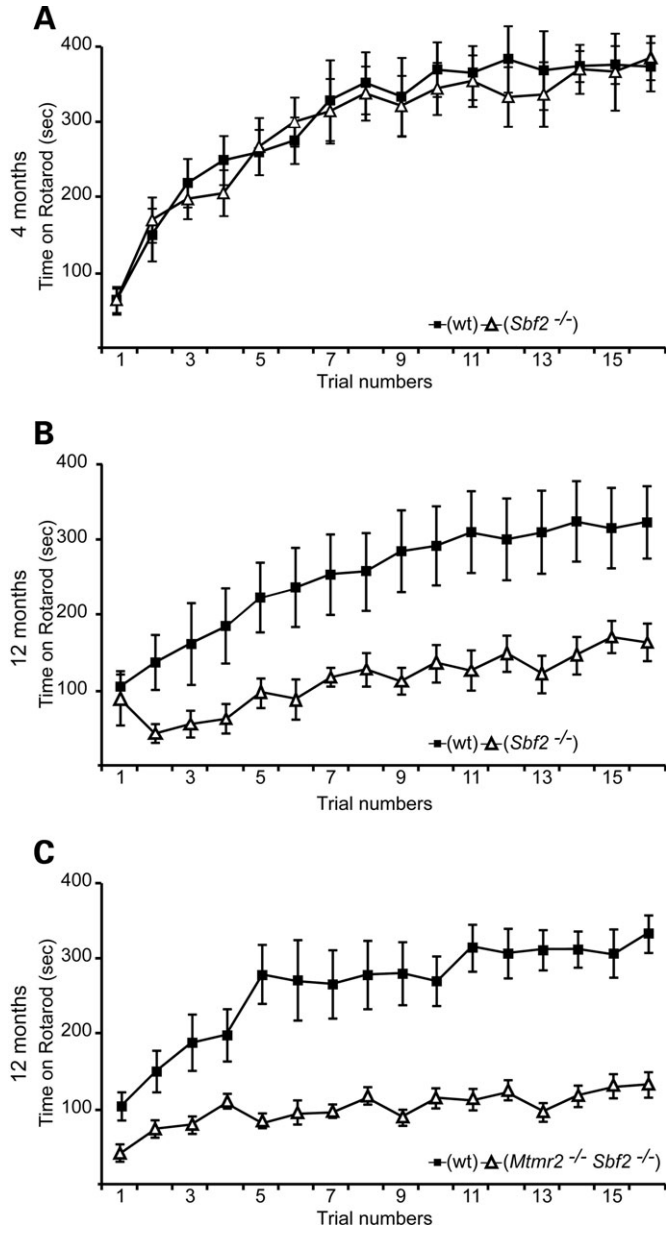

Figure 3. Rotarod analysis of wt, *Mtmr13/Sbf2-deficient (Sbf2−/−) and Mtmr2//Mtmr13/Sbf2-double deficient (Mtmr2−/− Sbf2−/−)* mice. Mice were tested four times per day on four consecutive days, and the time spent on the rotating rod was plotted versus the trial number. For statistical analysis a Students *t*-test was used. Error bars show the SEM. (**A**) Analysis of 4-months-old *Mtmr13/Sbf2-deficient (Sbf2−/−)* and wt control mice ($n = 6$). No significant difference between the two groups was detected. (**B**) Analysis of five 12-months-old *Mtmr13/Sbf2-deficient (Sbf2−/−)* mice and six wt control animals. Trials 2, 5, 6, 7 and 9-15 were significantly different for $P < 0.05$. (**C**) Analysis of *Mtmr2//Mtmr13/Sbf2-double deficient (Mtmr2−/− Sbf2−/−)* and wt control animals ($n = 8$). All trials were significantly different for $P < 0.05$.

Motor and sensory nerves are affected in *Mtmr13/Sbf2*-deficient mice

CMT4B2 is classified as a motor and sensory neuropathy. Thus, we analysed whether these mixed symptoms were reflected in pathological aberrations in both motor and sensory nerves. We chose to examine the ventral roots containing exclusively axons derived from motor neurons and dorsal roots for sensory axons. In both locations, the pathological hallmarks of myelin misfoldings were barely detectable at the age of 4 months (Fig. 8A and B), in contrast to the more distally (with respect to the neuronal cell bodies) located sciatic nerve (Fig. 6D) which contains both motor and sensory axons. These findings indicate that the pathology is more severe in distal compared to proximal parts of PNS nerves. At the age of 15 months, myelin misfoldings were prominently visible in ventral and dorsal roots suggesting that both motor and sensory nerves become affected in a progressive manner over time (Fig. 8C and D).

Complex structures of misfolded myelin in *Mtmr13/Sbf2*-deficient mice

In order to get some detailed insights into the fine structure of aberrant Schwann cell-axon units in our mutant mice, we performed ultrastructural analysis using electron microscopy. Figure 9 shows a collection of pictures to provide a sampling overview of the different aberrant structures that we have observed. The myelin misfoldings invariably originated from compacted myelin and showed an identical number of myelin lamellae in both myelin misfoldings and the myelin sheath they originated from (Fig. 9D, quantitative data not shown). Within myelin misfoldings, we observed normal compaction and periodicity of the myelin sheath. In general, the impression of pathological alterations was dominated by myelin outfoldings with strongly variable complexity (Fig. 9A–D). The most common formation consisted of one or multiple outfoldings of different size adjacent to a myelinated large calibre axon, and multiple outfoldings showed a tendency to form groups (Fig. 9C). Aberrant myelin loops were always ensheathed by the plasma membrane of the related Schwann cell (Fig. 9A). Myelin infoldings were also prominent. They usually presented as finger-like inversions of the myelin sheath (Fig. 9E) or circular inclusions within the myelinated nerve fibre (Fig. 9F). Entraining Schwann cell cytoplasm on their outer surface, they protrude far into the axon and displace the axoplasm (Fig. 9E). The formation of double circles (Fig. 9F and G) is most likely due to the retrograde inversion of a single infolding since, at higher magnifications, we observed axonal material in the gap between the inner and outer infolding. Alternatively, the nesting of two distinct infoldings may have led to the double-circle appearance.

On electrophysiological examination, older *Mtmr13/Sbf2*-deficient mice showed a reduction of the CMAP indicating axonal loss or damage. Thus, we also carefully looked for axonal pathology. Degeneration of whole Schwann cell-axon units (Fig. 9K and L) were not observed in young mutants, but were sporadically present at 4 months and rather frequent at 15th month. Lateral dislocation of the axon by myelin infoldings and vacuolar alteration of the axoplasm (Fig. 9I and J) was often observed. We occasionally found also myelinated nerve fibres not affected by myelin misfoldings but with a conspicuous widening of the periaxonal space (Fig. 9H).

The amazing complexity of myelin misfoldings and the consequences for the affected Schwann cell-axon units, however,

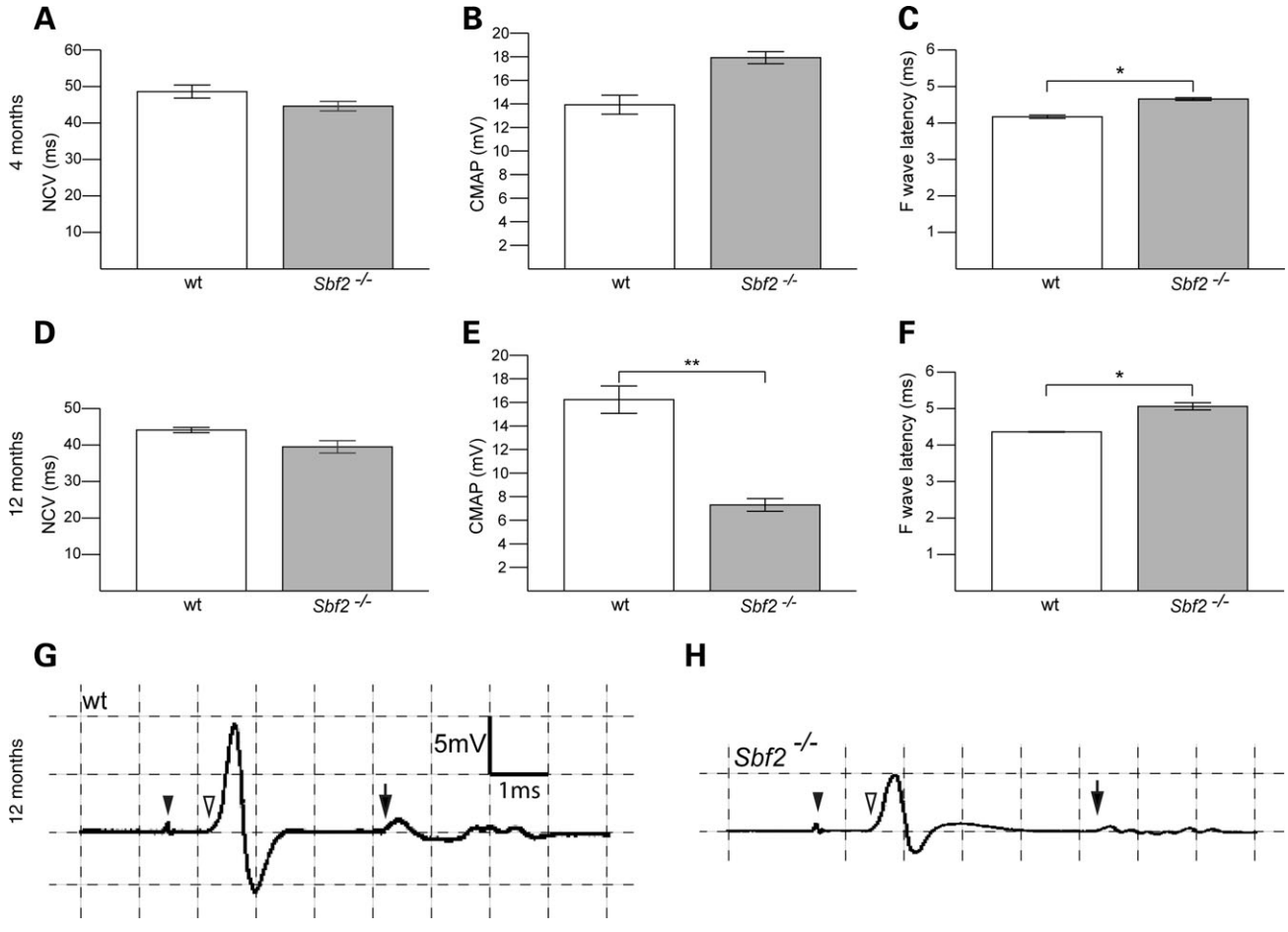

Figure 4. Motor nerve conduction studies of sciatic nerves of 4-month-old (**A**–**C**) and 12-month-old animals (**D**–**H**). Error bars indicate the SEM. (**A**) At 4 months of age, *Mtmr13/Sbf2-deficient (Sbf2−/−)* mice showed mild but not significant NCV slowing compared to wt mice ($n = 6$). (**B**) In comparison to wt animals, *Mtmr13/Sbf2-deficient (Sbf2−/−)* mice showed no significant difference in CMAP amplitudes at this age. (**C**) F-wave latency was slightly but significantly increased in *Mtmr13/Sbf2-deficient (Sbf2−/−)* mice compared to wt ($^*P < 0.05$ Student's *t*-test). (**D**) At the age of 12 months, *Mtmr13/Sbf2-deficient (Sbf2−/−)* mice showed still no significant NCV slowing compared to wt mice ($n = 8$). (**E**) In comparison to wt animals, *Mtmr13/Sbf2-deficient (Sbf2−/−)* mice showed now significantly reduced CMAP amplitudes ($^{**}P < 0.001$, Student's *t*-test; $n=8$). (**F**) The F-wave latency was slightly but significantly increased in *Mtmr13/Sbf2-deficient (Sbf2−/−)* mice compared to wt ($^*P < 0.05$ Student's *t*-test). (**G** and **H**) Representative recorded traces after stimulation at the (distal) ankle from 12-months-old wt and *Mtmr13/Sbf2-deficient (Sbf2−/−)* mice show profiles of CMAP. A filled arrowhead indicates the stimulus and a white arrowhead indicates the onset of the CMAP elicited. A black arrow indicates the beginning of the F-wave.

can be best appreciated on longitudinal sections (Fig. 9M–P). Complex myelin formations are preferentially, although not exclusively, located in the nodal and paranodal regions. At the same time, misfoldings contain axoplasm-like structures suggesting the entrainment of axonal parts during their formation (Fig. 9M and P). Occasionally, misfoldings of the myelin sheath had a larger diameter than the original nerve fibre, or lead to spatial disarrangement of the normal fibre anatomy like affecting the node of Ranvier (Fig. 9N). Relating these structural changes back to the molecular and cellular functions (and misfunctions in disease) of MTMR13/SBF2 will be a major challenge for the future. On a pure morphological level, the pathological observations in *Mtmr13/Sbf2*-deficient mice are very reminiscent of our observations in *Mtmr2*-deficient animals consistent with the biochemical finding suggesting a crucial role for a high-molecular complex containing both MTMR13/SBF2 and MTMR2 in the biology of myelinated peripheral nerves, possibly in the regulation of membrane trafficking.

DISCUSSION

We report the generation and analysis of the first animal model for the human neuropathy CMT4B2 by disruption of *Mtmr13/Sbf2* in mice. To our knowledge, this is also the first animal model for a genetically inherited human disease caused by mutations affecting an inactive member of the myotubularin phosphatase family. The aim of this study was three-fold. First, we wanted to provide the formal proof that mutations in *Mtmr13/Sbf2* are indeed causative for CMT4B2. Second, we anticipated that the generation of an animal model for this particular form of CMT will contribute critically to the dissection of the underlying disease mechanisms, especially with regard to the development and the progression of the disorder but also by providing appropriate means for further cell biological and biochemical analysis. Finally, recent reports relying on the analysis of appropriate CMT animal models have provided hopeful projections for treatment strategies encouraging the development of further refined animal models (25–28).

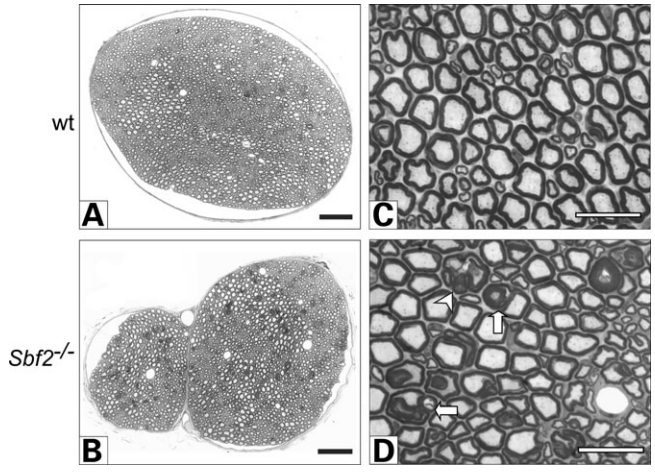

Figure 5. Histological analysis of cross sections of sciatic nerves at 4 months of age. Wt (**A**, **C**) and *Mtmr13/Sbf2-deficient (Sbf2−/−)* (**B**, **D**) mice were compared. *Mtmr13/Sbf2-deficient (Sbf2−/−)* mice show numerous nerve fibres with putatively redundant myelin loops scattered across the nerve section. Affected nerve fibres exhibit different morphologies including myelin sheath outfoldings and infoldings (white arrows in D), and likely degradation of the axon-Schwann cell unit (white arrowhead in D). Scale bars for A, B: 100 μm; for C, D: 25 μm.

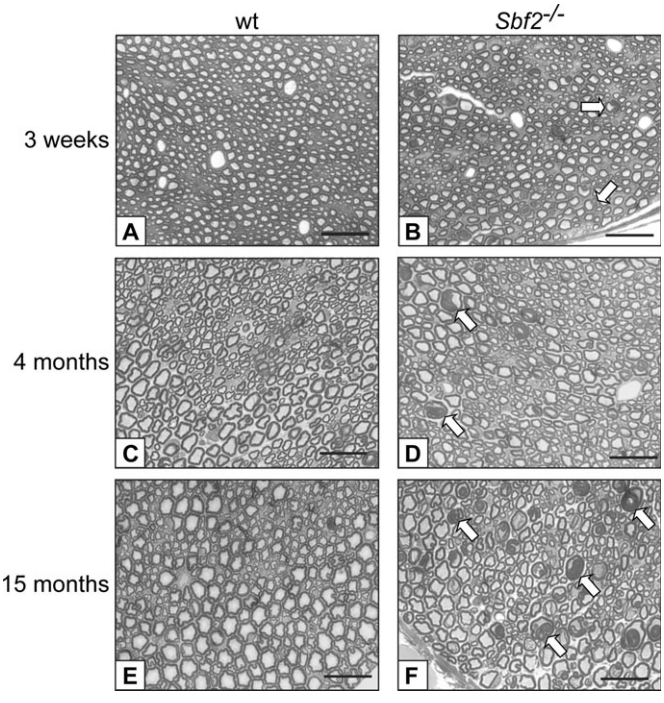

Figure 6. Time course of morphologic changes indicates a progressive neuropathy in *Mtmr13/Sbf2-deficient (Sbf2−/−)* mice. A qualitative and quantitative analysis of sciatic nerve cross section was performed at the age of 3 weeks, 4 months and 15 months. Three animals were analysed per age and genotype, and representative images are shown. At 3 weeks (**A** and **B**), mutant animals already show focally folded myelin (white arrows in B), ranging from mere 'budding' (oblique white arrow in B) to a major outfolding of the myelin sheath (horizontal white arrow in B). At 4 months (**C** and **D**) and at 15 months (**E** and **F**), mutant mice exhibit numerous nerve fibres with redundant myelin loops (oblique white arrows in D and F). Progression of the neuropathy is reflected by an increasing number of affected fibres, a higher morphological complexity of myelin abnormalities and signs of additional axonal degradation. Focal folding of the myelin sheath may be also observed, albeit very rarely, in wt littermates, possibly reflecting age-dependent dysmyelination. Scale bars: 25 μm.

Initial analysis of *Mtmr13/Sbf2*-deficient mice as animal models for CMT4B2 revealed behavioural deficits in the rotarod assay not in 4 months but in 12-month-old mice indicating significant motor impairments. This finding is consistent with the general clinical features of CMT4B2 patients that involve motor and sensory disturbances (11,12). Further analysis by light microscopy and ultrastructural analysis of peripheral nerves by electron microscopy showed prominent and complex myelin infoldings and outfoldings reminiscent of CMT4B2 (9). Our mouse model allowed us to follow the development of these pathological features in a temporal fashion by analysing peripheral nerves at different time points. Both the number and complexity of the unusual myelin figures increased gradually over time in a continuous fashion with little inter-animal variability. Some signs of axonal damage were also observed, in particular in older animals. Nevertheless, we did not find obvious evidence for primary demyelination and remyelination as judged from the lack of major Schwann cell onion bulb formations in the mouse mutant nerves up to the age of 15 months (last time point examined) and no decrease in myelin thickness. Consistent with these findings, we observed only minor signs of reduced NCV (prolonged F-wave latency). This appears to be in contrast to the strongly reduced NCV in CMT4B2 patients (9,12). Although the reason for this discrepancy is not yet clear, it should be noted that animal models for the related condition CMT4B1, associated with Mtmr2 deficiency, showed also much milder electrophysiological abnormalities compared to the corresponding human patients (14,15). It remains to be determined whether this feature is due to some specific mechanistic aspects of CMT4B-type neuropathies. Similarly, we did not observe a striking loss of myelinated large calibre axons in *Mtmr13/Sbf2*-deficient mice as has been reported based on qualitative assessments of sural nerve biopsies of CMT4B2 patients (9,12). Demyelination and in particular secondary axonal loss might be more pronounced in humans in these distally accentuated neuropathies due to basic physiological species differences that include much longer nerves and the longer life span of humans compared to mice (5). We found, however, a correlation between the rather poor performance of the mutants in the functional testing on the rotarod and the reduction of the CMAP amplitude. Since we did not observe major axonal loss, we favour the hypothesis that distal conduction block occurs in a significant proportion of fibres, possibly due to axonal constrictions by major myelin infoldings. Perinodal abnormalities may also lead to conduction block in the affected fibres resulting in reduced CMAP amplitudes.

The progressive formation of aberrant myelin outfoldings and infoldings is a robust feature caused by both MTMR2 and MTMR13/SBF2-deficiency in human and mice. This poses the major question how these abnormalities are generated and lead to disease. The first important conceptual point in this context concerns the determination of the cell type(s) which require the correct function of these proteins in a cell-autonomous or potentially non-cell autonomous

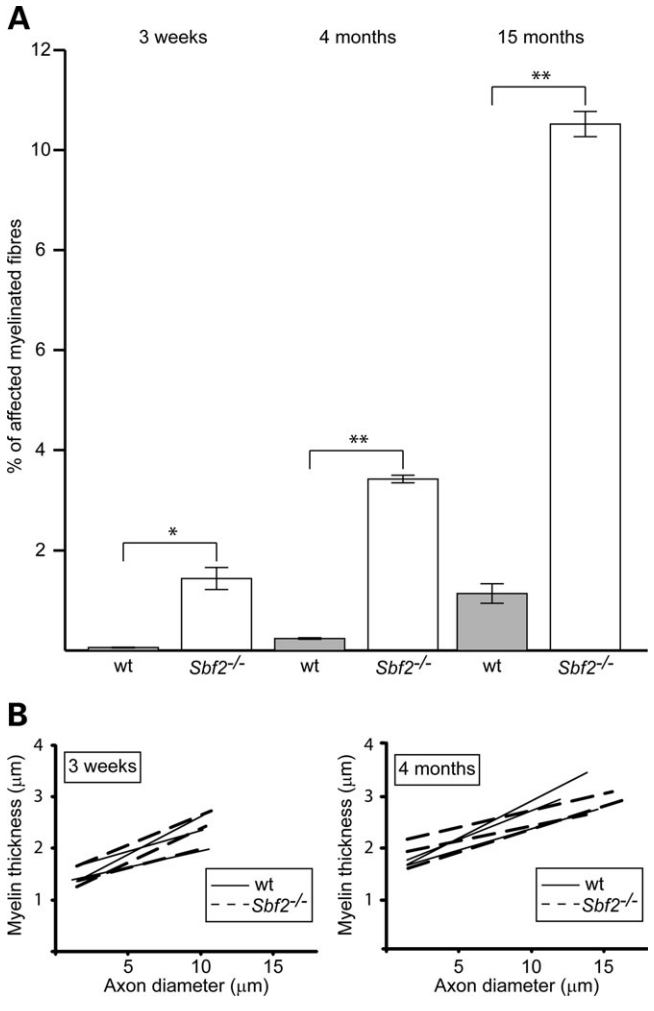

Figure 7. Quantification of myelin misfoldings, whole fibre morphometry and relation between axon diameter and myelin sheath thickness. (**A**) Quantification of myelinated fibres at 3 weeks, 4 months and 15th month of age. For each stage, the sciatic nerves were isolated from three mice per genotype. Two semithin sections per nerve, taken at an interval of 1.5 mm, were used for quantification. After the total number of fibres had been determined, the proportion of myelinated fibres exhibiting misfolded myelin was calculated. (**B**) Relation between axon diameter and myelin sheath thickness of 3-week- and 4-month-old mice. For each age, the sciatic nerves of three animals per genotype were analysed. Myelin thickness was determined and plotted as a function of the corresponding axon diameter. Each line represents the trend line for one mouse. Slope and intercept did not differ significantly between wt and *Mtmr13/Sbf2-deficient* ($Sbf2^{-/-}$) mice at either age. For statistical analysis, a Student's *t*-test was used (*, $P < 0.05$; **, $P < 0.001$). Error bars show the SEM.

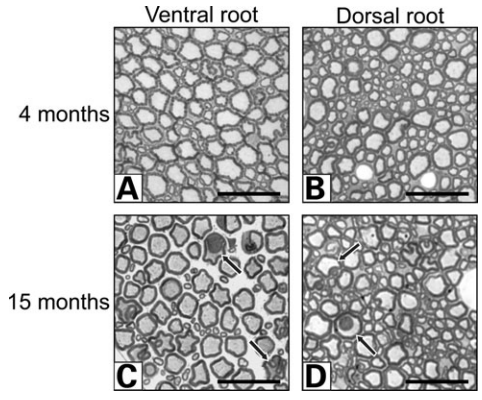

Figure 8. Involvement of proximal motor and sensory nerves in *Mtmr13/Sbf2-deficient* mice. Histological analysis of ventral and dorsal roots from mutant mice at four and 15 months of age. On cross sections from 4-month-old mutants (**A** and **B**), focally folded myelin is only scarcely present. At 15 months, both infoldings and outfoldings of the myelin sheath are present in dorsal and ventral roots (arrows in **C** and **D**), reflecting a progressive involvement of proximal nerves in the neuropathy. Scale bar for (A–D): 25 μm.

manner. Although it appears likely from the data presented here and other reports that myelinating Schwann cells are malfunctioning in CMT4B1 and CMT4B2, the close interactions between axon and Schwann cells require a careful direct experimental analysis. Using conditional gene targeting in the mouse, Bolis *et al*. (23) have elegantly shown that loss of MTMR2 is sufficient to cause the typical myelin abnormalities in a Schwann cell-autonomous manner. Complementary experiments will be necessary to answer this question also for MTMR13/SBF2.

Although it is not known in detail which signalling cascades are involved in the molecular pathogenesis of CMT4B1 and CMT4B2, the related processes involve regulation at various levels (20,22,29). MTMR13/SBF2 appears to act at least (i) as a regulator of the MTMR2 phosphatase activity, (ii) as a protector of the PI substrates, and (iii) as an adaptor regulating the localization of active MTMR2. Membrane PI-binding GRAM-PH and PH domains in MTMR2 as well as MTMR13/SBF2 play a major role in at least some of these processes, possibly by regulating vesicular and membrane trafficking in Schwann cells since loss of these proteins is associated with uncontrolled folding of myelin and CMT4B. Recently, mutations in the Rho-type GTPase guanine nucleotide exchange factor (GEF) *Frabin/FGD4* have been shown to be associated with CMT4H characterized by abundant myelin outfoldings (30,31). In addition to a RhoGEF (DH) domain, Frabin contains two PH domains and a presumably PI-binding FYVE domain. It is tantalizing to speculate that the presence of PI-binding domains in the disease-causing *MTMR2*, *MTMR13/SBF2* and *Frabin/FGD4* genes and the striking correlation with myelin outfoldings might be related to overlapping disease mechanisms. Further, how Dlg1/Sap97 and neurofilament light chain protein as described interaction partners of MTMR2 are involved in the disease process causing CMT4B remains to be determined (14,32).

In conclusion, we have generated an animal model for CMT4B2. In combination with the available *Mtmr2*-mutant mice, the *Mtmr13/Sbf2*-deficient animals provide valuable tools for future mechanistic studies in hereditary neuropathies characterized by myelin outfoldings and infoldings.

MATERIALS AND METHODS

Generation of *Mtmr13/Sbf2*$^{-/-}$ mice

The *Mtmr13/Sbf2*—mutant cell line (XH212) was obtained from MMRRC / BayGenomics ES Cell Clones (http://baygenomics.ucsf.edu/cgi-bin/BaySearch.py). Details for

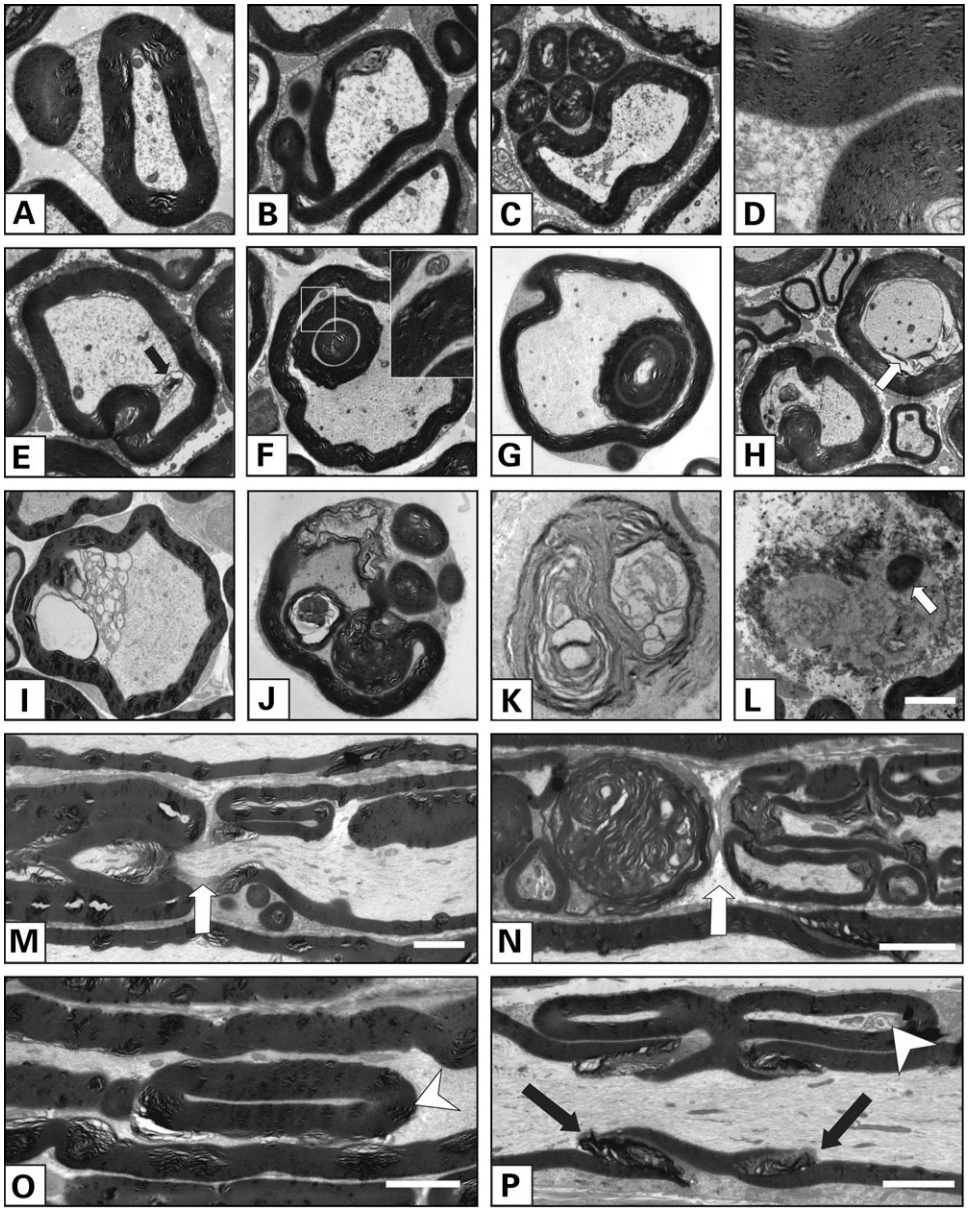

Figure 9. Electron microscopic analysis of focally folded myelin and axonal degeneration in sciatic nerve of *Mtmr13/Sbf2-deficient* mice. The figure shows a collection of different morphologies at age P21 (**A**–**D**), 4 months (**E**–**F**, **M**, **O**, **P**), and 15 months (**G**–**L**, **N**). Outfolding of the myelin sheath is the most frequent type of dysmyelination (A–C). Single or multiple redundant myelin loops are visible adjacent to the original myelinated fibre. The Schwann cell membrane surrounds both the outfoldings and the Schwann cell-axon unit they arise from. Simple outfoldings and the original myelin sheath share the same periodicity and number of lamellae (D). Infoldings of the myelin sheath may severely affect the axonal shape by leading to constriction of the axonal cytoplasm (arrow in E) or by forming extensions giving the cross-sectioned fibre a target-like appearance (F and G). The double circles in F and G likely reflect the retrograde inversion of infolded myelin loops. Note that the interspaces between the inner and outer infolding and the original myelin sheath show the structure of axonal cytoplasm (insert in F). Some fibres exhibit both infoldings and outfoldings (G). Apart from abnormalities of the myelin sheath, some fibres show disintegration or even degradation of the entire Schwann cell-axon unit. We observed widening of the periaxonal space (white arrow in H), vacuolar disruption of the inner myelin layers (I), compression and lateralization of the axon by massive infoldings (J) and various stages of axonal degeneration (K and L). The white arrow in L points to residual myelin. Longitudinal sections (M–P) revealed preferential location of myelin abnormalities in the nodal and paranodal segments (white arrow in M). Note that the aberrant myelin loops ensheath axonal processes and lead to massive disruption of the normal architecture of the node, which here is forced off the cutting plane (white arrow in N). Infoldings and outfoldings also occur in the internodal segment of the myelinated fibre (white arrowhead in **O**) or near the Schmidt-Lantermann incisures (arrows and white arrowhead in P). Scale bars for D: 1 μm, L–P: 5 μm.

gene-trap mutagenesis (33) in mouse embryonic stem cells can be found at http://baygenomics.ucsf.edu/protocols/index.html. The precise insertion of the gene-trap vector (pGT1lxf) in the ES cell genome was determined by Inverse PCR and DNA sequencing. The cell line was used for blastocyste injection (Institute of Laboratory Animal Science, University of Zürich) to obtain chimeric mice and these were crossed with C57Bl/6 mice. The offspring resulted in expected mendelian frequencies (wt: 26.1%; heterozygous: 49.2%; homozygous: 24.7%; $n = 412$).

Genotyping PCR

Tail genomic DNA was used for the genotype analysis. Primer pairs I and III were used to characterize the wt allele. Primer pairs II and III were used for the detection of the mutated allele. I: 5′-TCA GCA GCC AGG GAA CGG AGA C -3′. II: 5′-GGA GCA GAC AAG CCC GTC AGG-3′. III: 5′-AAG AA GGA AGA AAG ACA GTC CG-3′.

Protein expression analysis on mutant and wt sciatic nerves

Sciatic nerve tissue was dissected, frozen in liquid nitrogen, pulverized with a chilled mortar and pestle and dissolved in SDS gel sample buffer (34). Proteins were electophoresed on 10% SDS-polyacrylamide gels, transferred onto a Polyvinylidene fluoride (PVDF) membrane (Millipore), and immunoblotted with antibodies against Mtmr13/Sbf2 [1:500; rabbit polyclonal anti-peptide antibodies raised against the peptide CKNKLLRASAPGDWES (20)], Mtmr2 [1:500; rabbit polyclonal anti-peptide antibodies raised against the peptide CSTSHSENSVHTKSAS (20)], Dlg1/Sap97 (BD Transduction Laboratories; 1:1000) and beta-actin (Sigma; 1:5000). After incubation with goat anti-rabbit horseradish peroxidase-(Jackson Laboratories; 1:10000) or goat anti-mouse alkaline phosphatase-conjugated secondary antibodies (Promega; 1:10000), immunoreactive bands were visualized by West Pico Chemiluminescent Substrate (Pierce) or CDP-Star (Roche). Blots were quantified using ImageJ software (http://rsb.info.nih.gov/ij/) and normalized to the beta-actin signal

Rotarod test

Mice were placed on a rotarod apparatus (TSE Systems, Germany) and the time spent on the rotating rod, rotating from 4 to 40 rpm, was measured. Four trials per day, every 2 h, on four consecutive days were performed with a maximal trial length of 10 min.

Neurophysiology

Motor nerve conduction of sciatic nerves was investigated in anesthesized animals as described previously (35). CMAP and F-wave were recorded with needle electrodes in the foot muscles after supramaximal stimulation of the tibial nerve at the ankle and stimulation of the sciatic nerve at the sciatic notch. Statistical analysis was performed using Student's *t*-test.

Electron microscopy

Animals were anesthesized and sequentially perfused with 0.25 mg/ml heparin in 0.1 M PBS and a fixative solution containing 4% PFA and 2% glutaraldehyde in 0.1 M cacodylate buffer (pH 7.4). Sciatic nerves were dissected, postfixed for 24 h at 4°C, osmicated for 2 h in 2% osmium tetroxide, washed in distilled water several times, dehydrated in ascending acetone and embedded in Spurr's medium (36). Ninety nanometer ultrathin sections cut on an Ultracut E microtome (Reichert-Jung, Heidelberg, Germany) were mounted on copper grids and contrasted with uranyl acetate and lead citrate. Digital photographs were taken on a Philips EM 208 S transmission electron microscope using the iTEM® software (Olympus Soft Imaging Solutions, Muenster, Germany).

Morphometric analysis and quantification of focally folded myelin

Sciatic nerves from intracardially perfused animals were osmicated and embedded in Spurr's medium as described above. Semithin sections (0.5 μm) were stained with alkaline toluidine blue under standardized conditions to obtain identical results with regard to contrast and colour intensity. Semithin sections were visualized in a Leica DMRX microscope at 400-fold magnification, and a series of partially overlapping images covering the cross-sectional area was captured with a SPOT digital camera (Diagnostic Instruments, Sterling Heights, MI, USA). In order to obtain a composite image of the entire cross section, single images were pasted together using a Gaussian filter. Image processing and morphometric data collection were performed using the analySIS® software (Olympus Soft Imaging Solutions, Muenster, Germany). A macro was designed to meet the specific requirements of morphometric analysis. To discriminate axons and myelin sheaths, we defined a grey-scale threshold level for axon and myelin profiles. For each nerve fibre, both axon and myelin area were measured, and the diameter of axons and myelinated fibres were mathematically deduced from a circle of an equivalent area. Paranodes, Schwann cell nuclei, nerve fibres with focally folded myelin, and unmyelinated fibres were manually excluded from morphometry. We analysed two sciatic cross sections per animal (mutant and wt), and sections were taken from different levels 1.5 mm apart. For quantification of dysmyelinated nerve fibres, we determined the total number of fibres on each cross section, and the proportion of myelinated fibres showing focally folded myelin was calculated.

ACKNOWLEDGEMENTS

We thank Joke Nowitzki for excellent technical assistance and Ned Mantei for generous support.

FUNDING

This work has been supported by the Deutsche Forschungsgemeinschaft (DFGY048/3-1), the Swiss National Science Foundation, and the NCCR Neural Plasticity and Repair.

Conflict of Interest statement. The authors declare that they have no conflict of interest regarding this manuscript.

REFERENCES

1. Dyck, P.J., Chance, P., Lebo, R. and Carney, J.A. (1993) Hereditary motor and sensory neuropathies. Dyck, P.J., Thomas, P.K., Grffin, J.W., Low, P.A. and Poduslo, J.F. (eds). Peripheral Neuropathy, Philadelphia.

2. Niemann, A., Berger, P. and Suter, U. (2006) Pathomechanisms of mutant proteins in Charcot-Marie-Tooth disease. *Neuromolecular Med.*, **8**, 217–242.
3. Berger, P., Niemann, A. and Suter, U. (2006) Schwann cells and the pathogenesis of inherited motor and sensory neuropathies (Charcot-Marie-Tooth disease). *Glia*, **54**, 243–257.
4. Skre, H. (1974) Genetic and clinical aspects of Charcot-Marie-Tooth's disease. *Clin. Genet.*, **6**, 98–118.
5. Suter, U. and Scherer, S.S. (2003) Disease mechanisms in inherited neuropathies. *Nat. Rev. Neurosci.*, **4**, 714–726.
6. Zuchner, S. and Vance, J.M. (2006) Mechanisms of disease: a molecular genetic update on hereditary axonal neuropathies. *Nat. Clin. Pract. Neurol.*, **2**, 45–53.
7. Quattrone, A., Gambardella, A., Bono, F., Aguglia, U., Bolino, A., Bruni, A.C., Montesi, M.P., Oliveri, R.L., Sabatelli, M., Tamburrini, O. *et al.* (1996) Autosomal recessive hereditary motor and sensory neuropathy with focally folded myelin sheaths: clinical, electrophysiologic, and genetic aspects of a large family. *Neurology*, **46**, 1318–1324.
8. Gambardella, A., Bolino, A., Muglia, M., Valentino, P., Bono, F., Oliveri, R.L., Sabatelli, M., Brancolini, V., Van Broeckhoven, C., Romeo, G. *et al.* (1998) Genetic heterogeneity in autosomal recessive hereditary motor and sensory neuropathy with focally folded myelin sheaths (CMT4B). *Neurology*, **50**, 799–801.
9. Othmane, K.B., Johnson, E., Menold, M., Graham, F.L., Hamida, M.B., Hasegawa, O., Rogala, A.D., Ohnishi, A., Pericak-Vance, M., Hentati, F. *et al.* (1999) Identification of a new locus for autosomal recessive Charcot-Marie-Tooth disease with focally folded myelin on chromosome 11p15. *Genomics*, **62**, 344–349.
10. Bolino, A., Muglia, M., Conforti, F.L., LeGuern, E., Salih, M.A., Georgiou, D.M., Christodoulou, K., Hausmanowa-Petrusewicz, I., Mandich, P., Schenone, A. *et al.* (2000) Charcot-Marie-Tooth type 4B is caused by mutations in the gene encoding myotubularin-related protein-2. *Nat. Genet.*, **25**, 17–19.
11. Azzedine, H., Bolino, A., Taieb, T., Birouk, N., Di Duca, M., Bouhouche, A., Benamou, S., Mrabet, A., Hammadouche, T., Chkili, T. *et al.* (2003) Mutations in MTMR13, a new pseudophosphatase homologue of MTMR2 and Sbf1, in two families with an Autosomal recessive demyelinating form of Charcot-Marie-Tooth disease associated with early-onset glaucoma. *Am. J. Hum. Genet.*, **72**, 1141–1153.
12. Senderek, J., Bergmann, C., Weber, S., Ketelsen, U.P., Schorle, H., Rudnik-Schoneborn, S., Buttner, R., Buchheim, E. and Zerres, K. (2003) Mutation of the SBF2 gene, encoding a novel member of the myotubularin family, in Charcot-Marie-Tooth neuropathy type 4B2/11p15. *Hum. Mol. Genet.*, **12**, 349–356.
13. Bolino, A., Levy, E.R., Muglia, M., Conforti, F.L., LeGuern, E., Salih, M.A., Georgiou, D.M., Christodoulou, R.K., Hausmanowa-Petrusewicz, I., Mandich, P. *et al.* (2000) Genetic refinement and physical mapping of the CMT4B gene on chromosome 11q22. *Genomics*, **63**, 271–278.
14. Bolino, A., Bolis, A., Previtali, S.C., Dina, G., Bussini, S., Dati, G., Amadio, S., Del Carro, U., Mruk, D.D., Feltri, M.L. *et al.* (2004) Disruption of Mtmr2 produces CMT4B1-like neuropathy with myelin outfolding and impaired spermatogenesis. *J. Cell Biol.*, **167**, 711–721.
15. Bonneick, S., Boentert, M., Berger, P., Atanasoski, S., Mantei, N., Wessig, C., Toyka, K.V., Young, P. and Suter, U. (2005) An animal model for Charcot-Marie-Tooth disease type 4B1. *Hum. Mol. Genet.*, **14**, 3685–3895.
16. Robinson, F.L. and Dixon, J.E. (2006) Myotubularin phosphatases: policing 3-phosphoinositides. *Trends Cell Biol.*, **16**, 403–412.
17. Laporte, J., Bedez, F., Bolino, A. and Mandel, J.L. (2003) Myotubularins, a large disease-associated family of cooperating catalytically active and inactive phosphoinositides phosphatases. *Hum. Mol. Genet.*, **12** (Spec No. 2), R285–R292.
18. Berger, P., Bonneick, S., Willi, S., Wymann, M. and Suter, U. (2002) Loss of phosphatase activity in Myotubularin-Related-Protein-2 is associated with Charcot-Marie-Tooth disease type 4B1. *Hum. Mol. Genet*, **11**, 1569–1579.
19. Chow, C.Y., Zhang, Y., Dowling, J.J., Jin, N., Adamska, M., Shiga, K., Szigeti, K., Shy, M.E., Li, J., Zhang, X. *et al.* (2007) Mutation of FIG4 causes neurodegeneration in the pale tremor mouse and patients with CMT4J. *Nature*, **448**, 68–72.
20. Berger, P., Berger, I., Schaffitzel, C., Tersar, K., Volkmer, B. and Suter, U. (2006) Multi-level regulation of myotubularin-related protein-2 phosphatase activity by myotubularin-related protein-13/set-binding factor-2. *Hum. Mol. Genet.*, **15**, 569–579.
21. Begley, M.J., Taylor, G.S., Kim, S.A., Veine, D.M., Dixon, J.E. and Stuckey, J.A. (2003) Crystal structure of a phosphoinositide phosphatase, MTMR2: insights into myotubular myopathy and Charcot-Marie-Tooth syndrome. *Mol. Cell.*, **12**, 1391–1402.
22. Robinson, F.L. and Dixon, J.E. (2005) The phosphoinositide 3-phosphatase MTMR2 associates with MTMR13, a novel membrane-associated pseudophosphatase also mutated in type 4B Charcot-Marie-tooth disease. *J. Biol. Chem.*, **280**, 31699–31707.
23. Bolis, A., Coviello, S., Bussini, S., Dina, G., Pardini, C., Previtali, S.C., Malaguti, M., Morana, P., Del Carro, U., Feltri, M.L. *et al.* (2005) Loss of Mtmr2 phosphatase in Schwann cells but not in motor neurons causes Charcot-Marie-Tooth type 4B1 neuropathy with myelin outfoldings. *J. Neurosci.*, **25**, 8567–8577.
24. Thurnherr, T., Benninger, Y., Wu, X., Chrostek, A., Krause, S.M., Nave, K.A., Franklin, R.J., Brakebusch, C., Suter, U. and Relvas, J.B. (2006) Cdc42 and Rac1 signaling are both required for and act synergistically in the correct formation of myelin sheaths in the CNS. *J. Neurosci.*, **26**, 10110–10119.
25. Sahenk, Z., Nagaraja, H.N., McCracken, B.S., King, W.M., Freimer, M.L., Cedarbaum, J.M. and Mendell, J.R. (2005) NT-3 promotes nerve regeneration and sensory improvement in CMT1A mouse models and in patients. *Neurology*, **65**, 681–689.
26. Sereda, M.W., Meyer zu Horste, G., Suter, U., Uzma, N. and Nave, K.A. (2003) Therapeutic administration of progesterone antagonist in a model of Charcot-Marie-Tooth disease (CMT-1A). *Nat. Med.*, **9**, 1533–1537.
27. Khajavi, M., Shiga, K., Wiszniewski, W., He, F., Shaw, C.A., Yan, J., Wensel, T.G., Snipes, G.J. and Lupski, J.R. (2007) Oral curcumin mitigates the clinical and neuropathological phenotype of the Trembler-J mouse: A potential therapy for inherited neuropathies. *Am. J. Hum. Genet.*, **81**, 438–453.
28. Passage, E., Norreel, J.C., Noack-Fraissignes, P., Sanguedolce, V., Pizant, J., Thirion, X., Robaglia-Schlupp, A., Pellissier, J.F. and Fontes, M. (2004) Ascorbic acid treatment corrects the phenotype of a mouse model of Charcot-Marie-Tooth disease. *Nat. Med.*, **10**, 396–401.
29. Berger, P., Schaffitzel, C., Berger, I., Ban, N. and Suter, U. (2003) Membrane association of myotubularin-related protein 2 is mediated by a pleckstrin homology-GRAM domain and a coiled-coil dimerization module. *Proc. Natl Acad. Sci. USA*, **100**, 12177–12182.
30. Stendel, C., Roos, A., Deconinck, T., Pereira, J., Castagner, F., Niemann, A., Kirschner, J., Korinthenberg, R., Ketelsen, U.P., Battaloglu, E. *et al.* (2007) Peripheral nerve demyelination caused by a mutant Rho GTPase guanine nucleotide exchange factor, frabin/FGD4. *Am. J. Hum. Genet.*, **81**, 158–164.
31. Delague, V., Jacquier, A., Hamadouche, T., Poitelon, Y., Baudot, C., Boccaccio, I., Chouery, E., Chaouch, M., Kassouri, N., Jabbour, R. *et al.* (2007) Mutations in FGD4 Encoding the Rho GDP/GTP Exchange Factor FRABIN Cause Autosomal Recessive Charcot-Marie-Tooth Type 4H. *Am. J. Hum. Genet.*, **81**, 1–16.
32. Previtali, S.C., Zerega, B., Sherman, D.L., Brophy, P.J., Dina, G., King, R.H., Salih, M.M., Feltri, L., Quattrini, A., Ravazzolo, R. *et al.* (2003) Myotubularin-related 2 protein phosphatase and neurofilament light chain protein, both mutated in CMT neuropathies, interact in peripheral nerve. *Hum. Mol. Genet.*, **12**, 1713–1723.
33. Skarnes, W.C. (2000) Gene trapping methods for the identification and functional analysis of cell surface proteins in mice. *Methods Enzymol.*, **328**, 592–615.
34. Atanasoski, S., Notterpek, L., Lee, H.Y., Castagner, F., Young, P., Ehrengruber, M.U., Meijer, D., Sommer, L., Stavnezer, E., Colmenares, C. *et al.* (2004) The protooncogene Ski controls Schwann cell proliferation and myelination. *Neuron*, **43**, 499–511.
35. Zielasek, J., Martini, R. and Toyka, K.V. (1996) Functional abnormalities in P0-deficient mice resemble human hereditary neuropathies linked to P0 gene mutations. *Muscle Nerve*, **19**, 946–952.
36. Martini, R., Zielasek, J., Toyka, K.V., Giese, K.P. and Schachner, M. (1995) Protein zero (P0)-deficient mice show myelin degeneration in peripheral nerves characteristic of inherited human neuropathies. *Nat. Genet.*, **11**, 281–286.